ACS OMEGA

http://pubs.acs.org/journal/acsodf

Article

Iron(II) Phthalocyanine Adsorbed on Defective Graphenes: A Density Functional Study

Huimin Yin, Heyun Lin, Yongfan Zhang, and Shuping Huang*

Cite This: *ACS Omega* 2022, 7, 43915−43922

Read Online

ACCESS | Metrics & More | Article Recommendations | Supporting Information

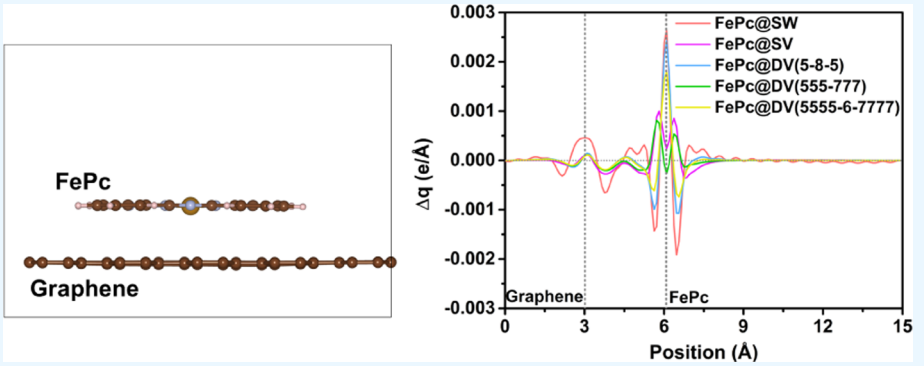

ABSTRACT: The adsorptions of iron(II) phthalocyanine (FePc) on graphene and defective graphene were investigated systematically using density functional theory. Three types of graphene defects covering stone-wales (SW), single vacancy (SV), and double vacancy (DV) were taken into account, in which DV defects included DV(5-8-5), DV(555-777), and DV(5555-6-7777). The calculations of formation energies of defects showed that the SW defect has the lowest formation energy, and it was easier for DV defects to form compared with the SV defect. It is more difficult to rotate or move FePc on the surface of defective graphenes than on the surface of graphene due to bigger energy differences at different sites. Although the charge analysis indicated the charge transfers from graphene or defective graphene to FePc for all studied systems, the electron distributions of FePc on various defective graphenes were different. Especially for FePc@SV, the d_{xy} orbital of Fe in the conduction band moved toward the Fermi level about 1 eV, and the d_{xz} of Fe in the valence band for FePc@SV also moved toward the Fermi level compared with FePc@graphene and other FePc@defective graphenes. Between the planes of FePc and defective graphene, the electron accumulation occurs majorly in the position of the FePc molecular plane for FePc@SW, FePc@DV(5-8-5), and FePc@DV(5555-6-7777) as well as FePc@graphene. However, electrons were accumulated on the upper and lower surfaces of the FePc molecular plane for FePc@SV and FePc@DV(555-777). Thus, the electron distribution of FePc can be modulated by introducing the interfaces of different defective graphenes.

1. INTRODUCTION

Organic optoelectronic materials have broad applications in the fields of electroluminescent devices, organic photovoltaic devices, and organic solar cells.[1,2] The research of these materials has always been a hot topic for scientists.[3−5] Metal phthalocyanines (MPcs), which form through the coordination of four isoindolyl nitrogen atoms with a central metal cation, have excellent optical and electrical properties and high chemical stability.[6,7] Researchers usually construct composites to maximize the utilization of MPcs.[8−11] Graphene, a two-dimensional (2D) structure with a single atomic layer composed of sp^2 hybrid carbon atoms with the honeycomb configuration, was first prepared by Novoselov et al. in 2004.[12,13] Due to its structural specificity, graphene has unique physicochemical properties, such as ultra-high specific surface area, excellent strength, and high mobility of electrons.[14−17] Graphene could be a promising ideal carrier owing to these unique properties.

Recently, iron phthalocyanine (FePc) and the FePc−carbon complex were prepared to investigate the catalytic activity in oxygen reduction reaction, revealing that FePc was a promising non-precious metal catalyst and the graphene carrier could significantly improve the stability, conductivity, and surface properties of FePc.[18−23] Actually, various defects were observed in graphene due to the presence of uncertainties in

Received: August 11, 2022
Accepted: November 8, 2022
Published: November 23, 2022

the material production process.[24−26] The electronic structure characteristics and optical properties of graphene may be affected by those defects. The defects in monolayer graphene were classified as point defects and one-dimensional defects by Banhart et al.[27] Stone-wales (SW), single vacancy (SV), double vacancy (DV), carbon and foreign adatoms, and substitutional impurities all belong to point defects. Although the consequences of the weak interactions between FePc and different substrates on the electronic structure of complex materials have been noticed by some workers,[28−31] systematic investigations are still scarce, especially the interaction between FePc and the 2D defective graphene.

Our previous work has carried out a density functional study of the adsorption of various MPc molecules (M = Cu, Fe, Zn, and Sn) on a perfect graphene monolayer.[32] It was found that the amount of charge transfer was the biggest in graphene−FePc. Thus, in this work, we focus on the electronic structure of FePc upon adsorption on various defective graphenes. Some physicochemical properties of defective graphene could be given to FePc by compounding it with various defective graphenes. Theoretically, we demonstrated that the interfacial electronic structure between FePc and graphene can be effectively modulated by the kinds of defects.

2. COMPUTATIONAL DETAILS

All calculations were performed with the density functional theory (DFT) using the spin-polarized version of the Vienna Ab initio Simulation Package.[33,34] The Perdew−Burke−Ernzerhof (PBE)[35] form of generalized gradient approximation (GGA) was used for the exchange−correlation functional, and the PAW[36] potentials were used to illustrate the electron−ion interaction. For FePc, the simplified GGA + U method proposed by Dudarev et al.,[37] of which the parameters U and J do not enter separately and only the difference $(U - J)$ is meaningful, was employed to describe the d electrons of Fe. Based on previous works,[32,38,39] we set $U - J = 4.5$ eV for the d orbital of Fe. The orthogonal supercell of graphene (a = 19.72 Å, b = 21.33 Å) containing 160 carbon atoms was employed for building defective graphenes. Periodic boundary conditions were used for all structures, and a distance of 15 Å along the z axis was applied to eliminate the interaction of stacked slabs. The 1 × 1 × 1 k-point was applied for structural optimization of graphene and defective graphene. The lattice parameters and atomic coordinates of all systems were fully relaxed with an energy cutoff of 400 eV. The energy convergence criterion for the self-consistent calculation was 10^{-4} eV and the determination of the optimal atomic positions were undertaken until the magnitude of the force acting on all atoms was less than 0.04 eV/Å. For the electronic property calculations, the Γ-centered 6 × 6 × 1 k-points were used. Grimme dispersion corrections (DFT-D2)[40] were applied for all adsorption systems to include the impact of van der Waals interaction.

The formation energy E_f of defective graphene is defined as

$$E_f = E_{d-graphene} + n \times E_c - E_{graphene} \quad (1)$$

where $E_{d\text{-}graphene}$ and $E_{graphene}$ represent the total energy of the defective graphene and the perfect graphene, respectively, n represents the number of defective atom, and E_c means the energy of a single C atom in the perfect graphene.

To evaluate the interaction of FePc with different defective graphenes, the adsorption energy is calculated as

$$E_a = E_{FePc@d-graphene} - E_{d-graphene} - E_{FePc} \quad (2)$$

where $E_{FePc@d\text{-}graphene}$, $E_{d\text{-}graphene}$, and E_{FePc} represent the total energies of FePc@defective-graphene systems, defective graphene, and FePc, respectively.

To further unravel the electron transfer patterns between the FePc plane and various defective graphenes, the charge density difference was calculated as follows.

$$\Delta\rho = \rho^{FePc@d-graphene} - \rho^{FePc} - \rho^{d-graphene} \quad (3)$$

where $\rho^{FePc@d\text{-}graphene}$, ρ^{FePc}, and $\rho^{d\text{-}graphene}$ represent the charge densities of FePc@defective-graphene, the FePc molecule, and defective graphene, respectively.

For more visualization of the amount of electron transfer, the planar-averaged charge density curves along the z-axis of FePc@defective-graphene systems were exhibited. One-dimensional differential charge density distribution curve along the z-axis can be defined as

$$\Delta q(z') = \int_{-\infty}^{+\infty}\int_{-\infty}^{+\infty} \Delta\rho(x, y, z')\mathrm{d}x\mathrm{d}y \quad (4)$$

3. RESULTS AND DISCUSSION

3.1. Structures of Defective Graphenes. Perfect graphene has a 2D crystalline structure consisting of honeycomb-like carbon hexagonal rings (Figure 1a) with the

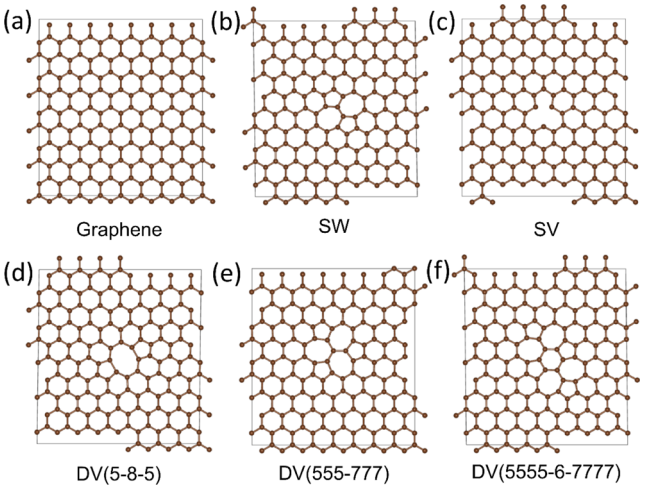

Figure 1. Top views of graphene (a) and various defective graphenes (b−f).

C−C bond of 1.42 Å and bond angles of 120.00°. The common point defects of graphene can be divided into three main categories: SW, SV, and DV.[27] The SW defective configuration is generated by the rotation of a pair of neighboring C atoms yielding adjacent two pentagonal and heptagonal rings (Figure 1b). The formation of a C vacancy in a carbon hexagonal ring can produce an SV defect (Figure 1c). The DV defects are built based on the SV defect with the loss of another C atom. Three kinds of DV defects are considered: DV(5-8-5), DV(555-777), and DV(5555-6-7777). DV(5-8-5) refers to the removal of a pair of neighboring C atoms yielding two pentagonal rings and one octagonal ring. Rotation of the C−C bond on one or both sides of the pair of C removed will generate DV(555-777) or DV(5555-6-7777) defects, accompanying the formation of three pentagonal rings and three heptagonal rings or one hexagonal ring, four pentagonal rings, and four heptagonal rings (Figure 1e,f). The electron

https://doi.org/10.1021/acsomega.2c05170
ACS Omega 2022, 7, 43915−43922

localization functions (ELFs) of various defects were shown in Figure S1. In the structures of graphene, SW, DV(5-8-5), DV(555-777), and DV(5555-6-7777) defective graphene, the electrons were localized between two C atoms and the adjacent C atoms are connected by covalent bonds. The formation of a C vacancy in SV yield three dangling bonds with bond angles of 112.75, 112.79, and 127.00°, respectively (details are in Figure S2). However, the ELF of the SV defect reveals that a pair of electrons will be localized between C78 and C82, forming a covalent bond with a bond length of 1.94 Å. Obviously, there was a dangling bond on the C81 atom with one lonely electron localization, which is consistent with the results observed experimentally by Meyer et al.[41] and Ugeda et al.[42] The total magnetic moment of SV-graphene is 1.19 μ_B, which is mainly localized on the dangling bond.

The calculated formation energies of various defects in graphene are listed in Table 1. The calculated formation energy of the SW defect in graphene is 4.45 eV, a bit larger than the one for the SiC monolayer.[43] However, it is smaller than those reported in the literature for a monolayer of graphite (4.8 eV by GGA and 5.2 eV by local density approximation),[44] which is mainly due to the different concentration of the SW defect, that is, different sizes of lattice cells used in the calculations. The SV defect has a much higher formation energy (7.63 eV) than the SW defect, indicating that it is easier for the SW defect to form in experiments. The calculated formation energy of the SV defect is close to the reported value (7.78 eV).[45] The average formation energies for each C vacancy in DV defects (3.09 ∼ 3.37 eV) are much lower than the one in the SV defect. Therefore, the DV defects are thermodynamically more favorable than the SV defect. Among the DV defects, DV(5-8-5) has the highest formation energy and DV(5555-6-7777) has the lowest formation energy. As observed by Kotakoski et al.[26] using an electron microscope, the rotation of C−C based on the DV(5-8-5) defect results in more configurations of DV(5555-6-7777) than those of DV(555-777).

Table 1. Calculated Formation Energies of Various Defects in Graphene

defects	formation energy (eV)
SW	4.45
SV	7.63
DV(5-8-5)	6.74
DV(555-777)	6.35
DV(5555-6-7777)	6.17

The density of states (DOSs) of graphene and defective graphenes are shown in Figure 2. We can clearly see the Dirac point overlapping with the Fermi energy level in the perfect graphene (Figure 2a). Defects in graphene affect the electronic properties significantly due to the p_z-orbital overlap altered in the vicinity of structural defects. The spin polarization occurs in the SV defect due to the presence of dangling bonds where the electrons were not completely paired (Figure 2c). No magnetism was present in other defects. Due to the symmetry breaking, the formation of band gaps was seen in the SW, DV(5-8-5), and DV(5555-6-7777) defects. The band gap opening in SW-graphene agrees with the results of Peng et al.[46] The Dirac point moved toward a higher energy (around 0.5 eV) in DV(555-777) defective graphene. The DOSs at the Fermi level increase for SV, which is mainly localized at the dangling bond. The result of the SV defect is consistent with the protrusion in scanning tunneling microscope images in experiments.[42]

3.2. Structures and Electronic Properties of FePc Adsorbed on Graphene and Defective Graphenes. We first focus our attention to the adsorption of FePc on the perfect graphene. Three different representative sites (Figure

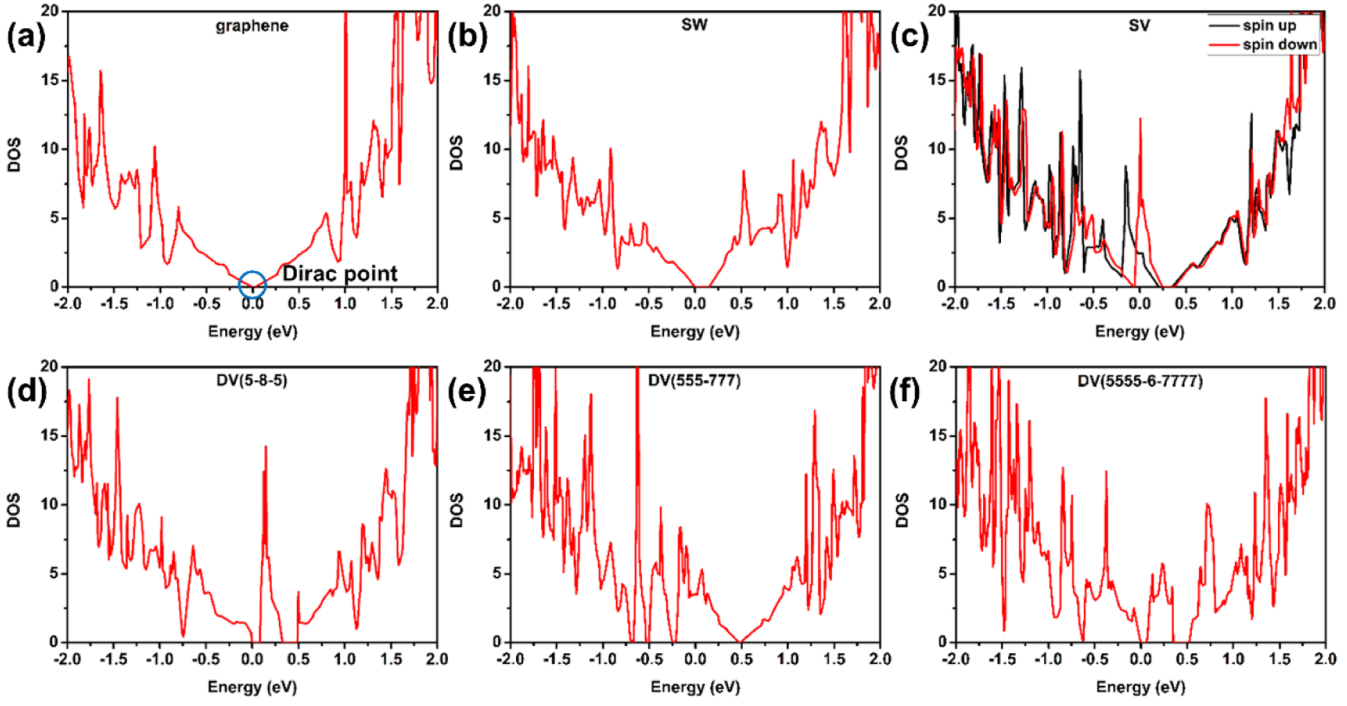

Figure 2. Total DOSs of (a) graphene and (b−f) defective graphenes. The black and red curves represent spin-up (α spin) and spin-down (β spin), respectively.

https://doi.org/10.1021/acsomega.2c05170
ACS Omega 2022, 7, 43915−43922

S3) were considered for all adsorptions with the center of the FePc atop a carbon atom (t), at the bridge site of C−C bond (b), and the hollow site of the carbon polygonal ring (h). Table 2 lists the adsorption energies of FePc at different sites

Table 2. Adsorption Energies E_a of FePc at Different Sites on Graphene

adsorption sites	E_a (eV)
top	−2.28
bridge	−2.33
hollow	−2.30

on graphene. The difference between them is small, within 0.05 eV. The bridge site of graphene is the most stable adsorption site for FePc, with an adsorption energy of −2.33 eV. For the bridge site of FePc@graphene (Figure S4), we considered the rotations of FePc on graphene and optimized the structure of FePc@graphene by rotating FePc 15, 30, 45, 60, 75, and 90° clockwise around the *c*-axis with Fe as the center, respectively, and the calculated relative energies are also shown in Figure S4. The difference in energies between them for FePc@graphene is also small, indicating that it is easy to move FePc on the surface of graphene. In the most stable configuration, the average distance between FePc to graphene (Fe atom to graphene carbon atom) is 3.13 Å. Rumpling of the carbon atom of graphene was 0.14 Å, which has also been calculated in our previous work.[32] For comparison with defective graphene, we still show the DOS and charge density difference of FePc@graphene in Figure S5. The band structure of graphene near the Dirac point is not appreciably affected after the adsorption of FePc, and the transfer of electrons from graphene to FePc can be clearly observed. An obvious loss of electrons occurs from 3.3 to 4.3 Å, with subsequent accumulation at about 5.1−6.0 Å.

All sites nearby the defects are considered to determine the most stable site for the adsorption of FePc on defective graphenes, as shown in Figure S6. The energy differences between different adsorption sites on defective graphenes are much bigger than that on graphene. Figure S7 shows the optimal adsorption sites of FePc on different defective graphenes. The results show that FePc prefers to adsorb at the bridge sites near the defects, except for DV(5-8-5). For the most stable adsorption site of FePc@defective graphenes (Figure S7), we also considered the rotations of FePc on defective graphenes and optimized the structure of FePc@defective graphenes by rotating FePc 15, 30, 45, 60, 75, and 90° clockwise around the *c*-axis with Fe as the center, respectively, and the calculated relative energies are shown in Figure 3. The differences in energies during the rotation are larger in defective graphenes, indicating that it is more difficult to rotate FePc on the surface of defective graphenes than on the surface of graphene.

The average distance, adsorption energy, and rumpling of a carbon atom of defective graphene for the optimal stable adsorption configurations of FePc@defective-graphene are displayed in Table 3. For all adsorptions, FePc was floating around 3.1 Å above the defective graphene. The adsorption energies for FePc@SW, FePc@SV, FePc@DV(5-8-5), FePc@DV(555-777), and FePc@DV(5555-6-7777) are −2.36, −2.26, −2.27, −2.28, and −2.30 eV, respectively. The defects have little effect on the adsorption energies. Rumplings of carbon atom in defective graphenes and FePc@defective-graphene are

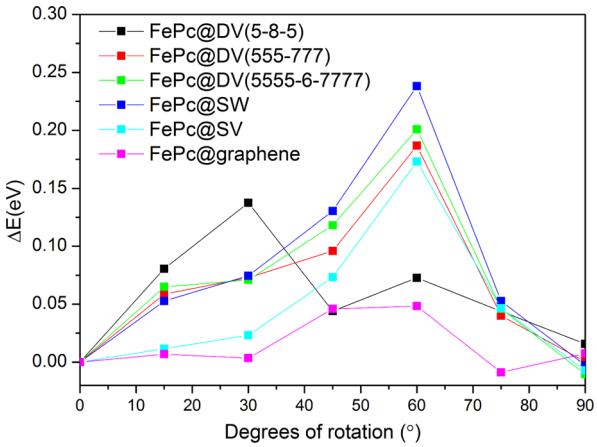

Figure 3. Relative energies for the rotation of FePc on graphene and defective graphenes at the most stable adsorption site. FePc was rotated 15, 30, 45, 60, 75, and 90° clockwise around the *c*-axis with Fe as the center.

exhibited in Tables S1 and 3. The rumple in defective graphene is almost negligible except for SV-graphene, while their rumplings are obvious after the adsorption of FePc. In comparison with FePc@graphene, a slight increase of the rumple in defective graphene after the adsorption of FePc was found. However, the situation of FePc@SV is a bit different. The Δd_C of SV-graphene was 0.02 Å. Following the adsorption of FePc, the Δd_C became 0.04 Å, which is much smaller compared with that of other defective graphenes. This might be caused by the presence of the dangling bond.

The change of magnetic moment of Fe in FePc@defective-graphene was also evaluated. The calculated magnetic moment of Fe in FePc is about 2.0 μ_B, and Fe is in an intermediate spin state, which is verified by previous calculations and experiments.[47] Table 3 shows that the magnetic moments of Fe calculated by PBE + *U* remained unchanged after the adsorption of graphene or defective graphenes, which is consistent with the calculation of Haldar et al.[48] The total magnetic moment of FePc@SV is about 1.0 μ_B higher than those of others due to the dangling bond in SV-graphene.

Hirshfeld charge analysis[49] was performed to obtain further insights into the charge transfer in the adsorption process. Table S2 lists the sums of Hirshfeld charges of various graphenes (graphene and defective graphenes) and FePc in the complex systems. The charge analysis indicated the charge transfers from graphene or defective graphene to FePc. The amount of the transferred charge is almost not related to the adsorption energy, which is similar to the previous result of Li adsorption on SiC surfaces.[50]

Figure 4 shows the calculated DOSs for the most stable FePc@graphene and FePc@defective-graphene using the PBE + *U* functional. All studied composite materials become magnetic, producing different spin-up and spin-down densities of states due to the adsorption of FePc. For FePc@graphene, the states around the Dirac point of graphene are not significantly affected, and the gap of graphene does not open. The small band gaps in SW, DV(5-8-5), and DV(5555-6-7777) defective graphenes were still preserved after the adsorption of FePc. For SV-graphene, the small peaks at the Fermi level which come from the dangling bond move toward conduction bands after the adsorption of FePc. The new peaks at the bottom of the conduction bands and the top of the

https://doi.org/10.1021/acsomega.2c05170
ACS Omega 2022, 7, 43915−43922

Table 3. Average Distance d, Adsorption Energy E_a, Rumpling of Carbon Atom Δd_C, and Magnetic Moments for FePc@graphene and FePc@defective-Graphene.

	d (Å)[a]	E_a (eV)	Δd_C (Å)[b]	magnetic moment of Fe (μ_B)	total magnetic moment (μ_B)
FePc				2.03	1.95
FePc@graphene	3.13	−2.33	0.14	2.03	1.91
FePc@SW	3.13	−2.36	0.19	2.03	1.92
FePc@SV	3.13	−2.26	0.04	2.04	3.11
FePc@DV(5-8-5)	3.11	−2.27	0.17	2.04	1.93
FePc@DV(555-777)	3.10	−2.28	0.16	2.04	1.93
FePc@DV(5555-6-7777)	3.11	−2.30	0.15	2.04	1.93

[a]The average distance of an Fe atom to a graphene carbon atom. [b]The distance of the highest C and the lowest C of graphene or defective graphene in FePc@graphene orFePc@defective-graphene.

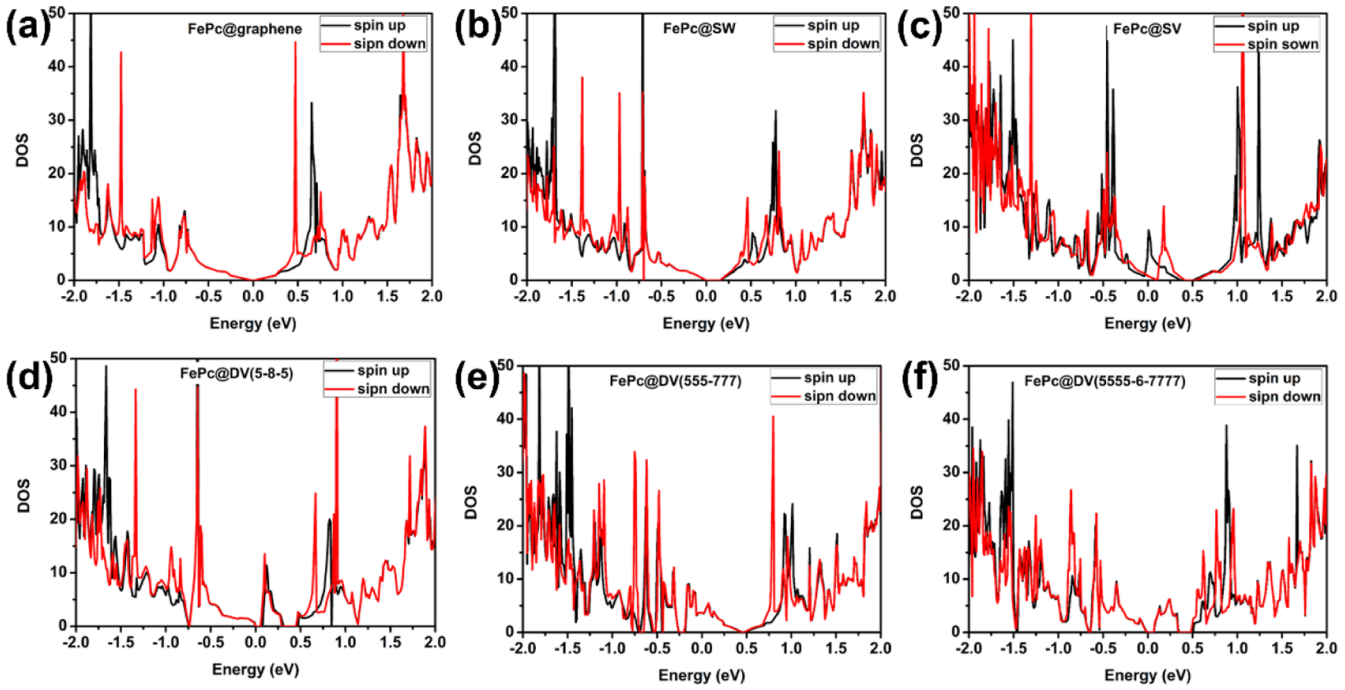

Figure 4. DOSs of (a) FePc@graphene, (b) FePc@SW, (c) FePc@SV, (d) FePc@DV(5-8-5), (e) FePc@DV(555-777), and (f) FePc@DV(5555-6-7777). The black and red curves represent spin-up (α spin) and spin-down (β spin), respectively.

valence bands in the composite system come from the contribution of FePc. Figure S8 shows the partial DOSs of Fe in the most stable FePc@graphene and FePc@defective-graphene by PBE + U. The positions of d_{xy} and d_{xz} of Fe for FePc@SV differs significantly from the ones in FePc@graphene and other FePc@defective-graphenes. The d_{xy} of Fe in the conduction band for FePc@SV move toward the Fermi level about 1 eV, and the d_{xz} of Fe in the valence band for FePc@SV also move toward the Fermi level.

The charge density differences of FePc@defective-graphene are shown in Figure 5a−e, and the planar-averaged charge density along the z-axis of FePc@defective-graphene is shown in Figure 5f. A complex rearrangement of the charge density occurred in the FePc@defective-graphene systems. For FePc@SV and FePc@DV(555-777), they have similar charge transfer patterns with the loss of electrons at the ranges of 2.0−2.8 and 3.4−5.5 Å and electron accumulation from 5.5 to 6.4 Å. Although the charge accumulation declines in the FePc molecular plane, the whole is in a state of charge accumulation in the range of 5.5 to 6.4 Å for FePc@SV and FePc@DV(555-777). For FePc@DV(5-8-5) and FePc@DV(5555-6-7777), the electron accumulation mainly takes place at 6.0 Å. For FePc@SW, the electron accumulates around 3.0, 5.3, and 6.0 Å, with the maximum peak at 6.0 Å. However, there is a reversal with a maximum electron loss at 5.6 and 6.5 Å. For different FePc@defective-graphenes, the most significant differences can be observed in the electron transfer patterns at 5.4−6.7 Å. For FePc@SV and FePc@DV(555-777), the charges start to accumulate as they get closer to the FePc molecular plane, and they reach the largest values on the upper and lower surfaces of the FePc molecule (at the positions of 5.8 and 6.3 Å) but decrease in the FePc plane (at the position of 6.0 Å). For FePc@SW, FePc@DV(5-8-5), and FePc@DV(5555-6-7777), the electron loss remains significant as the position (at the position of 5.6 Å) gets closer to the FePc molecular plane, yet the electron accumulation reaches a maximum value in the FePc molecular plane (at the position of 6.0 Å). Thus, the electron distribution around FePc can be regulated by its adsorption on various defective graphenes.

4. CONCLUSIONS

In this paper, the interaction between iron(II) phthalocyanine and defective graphene, such as SW, SV, DV(5-8-5), DV(555-777), and DV(5555-6-7777), was investigated based on first-

https://doi.org/10.1021/acsomega.2c05170
ACS Omega 2022, 7, 43915−43922

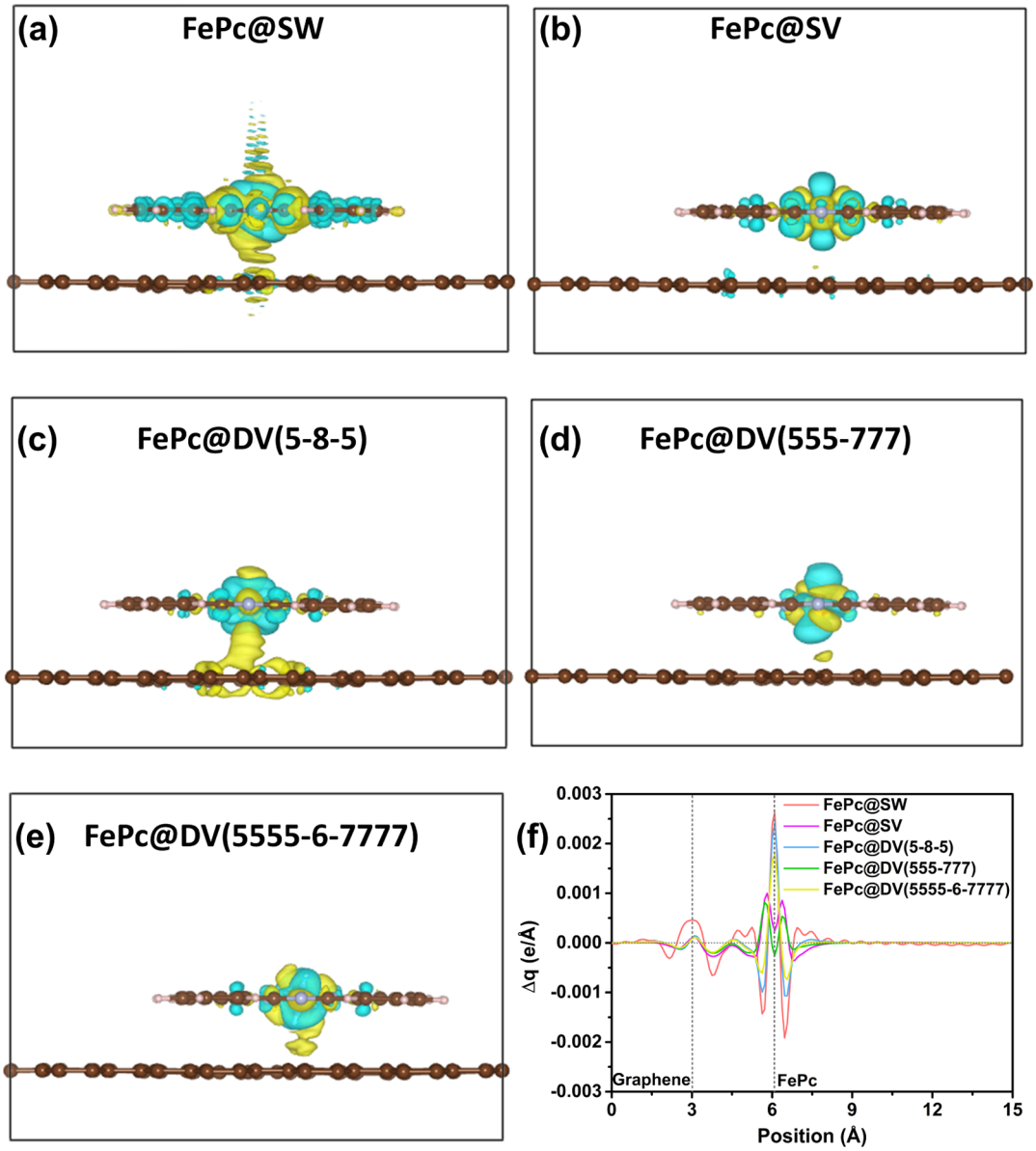

Figure 5. (a−e) Side views of charge density differences of FePc@defective-graphene. (f) Planar-averaged charge density along the *z*-axis of FePc@defective-graphene. The yellow (blue) isosurface indicates charge accumulation (depletion) density. The gray dotted line at 3 Å is the position of defective graphene, and the gray dotted line at about 6 Å is the position of the FePc plane. The isosurface level is set to 0.001 e/Å^3.

principles calculations. Among these five graphene defects, the formation energy of the SW defect was the lowest, and the DV defects were easier to form compared to the SV defect. The comparison of the adsorption of FePc at different sites on defective graphenes indicated that FePc preferred to float with Fe on the top of the edge of the defects in graphene. The Hirshfeld charge analysis showed the charge transfers from graphene or defective graphene to FePc, but the charge transfer patterns between FePc and defective graphene were diverse in different adsorption systems. Between the FePc plane and defective graphene plane of the adsorption systems, the electron accumulation occurs majorly in the position of the FePc molecular plane for FePc@SW, FePc@DV(5-8-5), and FePc@DV(5555-6-7777) as well as FePc@graphene. However, electrons were accumulated on the upper and lower surfaces of the FePc molecular plane for FePc@SV and FePc@DV(555-777) systems. The DOS calculations showed that the energy levels of some d orbitals changed after the adsorption of FePc on graphene or defective graphene. These discrepancies might be used to modulate the electrons distribution of FePc.

■ ASSOCIATED CONTENT

Supporting Information

The Supporting Information is available free of charge at https://pubs.acs.org/doi/10.1021/acsomega.2c05170.

Rumpling of the carbon atom Δd_C of optimized defective graphene; sum of Hirshfeld charges of various graphenes and FePc in complex systems; ELFs of graphene and defective graphenes; dangling bond of the SV defect and corresponding bond lengths and angles; three representative sites: top, bridge, and hollow; relative energies of different configurations by rotating the FePc of FePc@graphene clockwise around the *c*-axis with Fe as the center; side view of charge density difference and planar average charge density along the *z*-

https://doi.org/10.1021/acsomega.2c05170
ACS Omega 2022, 7, 43915−43922

axis of FePc@graphene; different adsorption sites of FePc on defective graphene; top views of FePc and the most stable adsorption sites of different defective graphenes; and PDOS of Fe in FePc@graphene and different defective graphenes (PDF)

AUTHOR INFORMATION

Corresponding Author

Shuping Huang − *College of Chemistry, Fuzhou University, Fuzhou, Fujian 350108, P. R. China; Fujian Provincial Key Laboratory of Electrochemical Energy Storage Materials, Fuzhou, Fujian 350108, P. R. China;* orcid.org/0000-0003-4815-1863; Email: huangshp@gmail.com

Authors

Huimin Yin − *College of Chemistry, Fuzhou University, Fuzhou, Fujian 350108, P. R. China*

Heyun Lin − *College of Chemistry, Fuzhou University, Fuzhou, Fujian 350108, P. R. China*

Yongfan Zhang − *College of Chemistry, Fuzhou University, Fuzhou, Fujian 350108, P. R. China;* orcid.org/0000-0003-3475-0937

Complete contact information is available at: https://pubs.acs.org/10.1021/acsomega.2c05170

Notes

The authors declare no competing financial interest.

ACKNOWLEDGMENTS

S.H. acknowledges the financial support from the National Natural Science Foundation of China (21703036) and the Natural Science Foundation of Fujian Province (2021J01547).

REFERENCES

(1) Yang, F.; Cheng, S.; Zhang, X.; Ren, X.; Li, R.; Dong, H.; Hu, W. 2D Organic Materials for Optoelectronic Applications. *Adv. Mater.* **2018**, *30*, 1702415.

(2) Coe, S.; Woo, W.-K.; Bawendi, M.; Bulović, V. Electroluminescence from single monolayers of nanocrystals in molecular organic devices. *Nature* **2002**, *420*, 800.

(3) Ge, J.; Fan, L.; Rao, A. M.; Zhou, J.; Lu, B. Surface-substituted Prussian blue analogue cathode for sustainable potassium-ion batteries. *Nat. Sustain.* **2022**, *5*, 225−234.

(4) Hu, Y.; Fan, L.; Rao, A. M.; Yu, W.; Zhuoma, C.; Feng, Y.; Qin, Z.; Zhou, J.; Lu, B. Cyclic-anion salt for high-voltage stable potassium-metal batteries. *Natl. Sci. Rev.* **2022**, *9*, nwac134.

(5) Li, J.; Hu, Y.; Xie, H.; Peng, J.; Fan, L.; Zhou, J.; Lu, B. Weak Cation-Solvent Interactions in Ether-Based Electrolytes Stabilizing Potassium-ion Batteries. *Angew. Chem., Int. Ed.* **2022**, *134*, No. e202208291.

(6) Nguyen, T. Q.; Escaño, M. C. S.; Kasai, H. Nitric Oxide Adsorption Effects on Metal Phthalocyanines. *J. Phys. Chem. B* **2010**, *114*, 10017.

(7) Yoshida, H.; Tsutsumi, K.; Sato, N. Unoccupied electronic states of 3d-transition metal phthalocyanines (MPc: M=Mn, Fe, Co, Ni, Cu and Zn) studied by inverse photoemission spectroscopy. *J. Electron Spectrosc. Relat. Phenom.* **2001**, *121*, 83.

(8) Dou, W.; Huang, S.; Zhang, R. Q.; Lee, C. S. Molecule−substrate interaction channels of metal-phthalocyanines on graphene on Ni(111) surface. *J. Chem. Phys.* **2011**, *134*, 094705.

(9) Scardamaglia, M.; Lisi, S.; Lizzit, S.; Baraldi, A.; Larciprete, R.; Mariani, C.; Betti, M. G. Graphene-Induced Substrate Decoupling and Ideal Doping of a Self-Assembled Iron-phthalocyanine Single Layer. *J. Phys. Chem. C* **2013**, *117*, 3019.

(10) Lei, S.; Feng, W.; Li, B.; Li, Q.; Zhao, A.; Wang, B.; Yang, J.; Hou, J. G. Orbital-selective single molecule rectifier on graphene-covered Ru(0001) surface. *Appl. Phys. Lett.* **2013**, *102*, 163506.

(11) Lei, Y.; Zhao, R.; Hu, G.; Yang, X.; Liu, X. Electromagnetic, microwave-absorbing properties of iron-phthalocyanine and its composites based on phthalocyanine polymer. *J. Mater. Sci.* **2012**, *47*, 4473.

(12) Novoselov, K. S.; Geim, A. K.; Morozov, S. V.; Jiang, D.; Zhang, Y.; Dubonos, S. V.; Grigorieva, I. V.; Firsov, A. A. Electric Field Effect in Atomically Thin Carbon Films. *Science* **2004**, *306*, 666.

(13) Tian, W.; Li, W.; Yu, W.; Liu, X. A Review on Lattice Defects in Graphene: Types, Generation, Effects and Regulation. *Micromachines* **2017**, *8*, 163.

(14) Castro Neto, A. H.; Guinea, F.; Peres, N. M. R.; Novoselov, K. S.; Geim, A. K. The electronic properties of graphene. *Rev. Mod. Phys.* **2009**, *81*, 109.

(15) Geim, A. K.; Novoselov, K. S. The rise of graphene. *Nat. Mater.* **2007**, *6*, 183.

(16) Lee, C.; Wei, X.; Kysar, W.; Hone, J. Measurement of the Elastic Properties and Intrinsic Strength of Monolayer Graphene. *Science* **2008**, *321*, 385.

(17) Tian, W.; Zhang, X.; Chen, Z.; Ji, H. A Review of Graphene on NEMS. *Recent Pat. Nanotechnology* **2016**, *10*, 3.

(18) Chen, K.; Liu, K.; An, P.; Li, H.; Lin, Y.; Hu, J.; Jia, C.; Fu, J.; Li, H.; Liu, H.; Lin, Z.; Li, W.; Li, J.; Lu, Y.-R.; Chan, T.-S.; Zhang, N.; Liu, M. Iron phthalocyanine with coordination induced electronic localization to boost oxygen reduction reaction. *Nat. Commun.* **2020**, *11*, 4173.

(19) Wang, Y.; Yuan, H.; Li, Y.; Chen, Z. Two-dimensional iron-phthalocyanine (Fe-Pc) monolayer as a promising single-atom-catalyst for oxygen reduction reaction: a computational study. *Nanoscale* **2015**, *7*, 11633.

(20) Arul, A.; Pak, H.; Moon, K. U.; Christy, M.; Oh, M. Y.; Nahm, K. S. Metallomacrocyclic−carbon complex: A study of bifunctional electrocatalytic activity for oxygen reduction and oxygen evolution reactions and their lithium-oxygen battery applications. *Appl. Catal., B* **2018**, *220*, 488.

(21) Jiang, Y.; Lu, Y.; Lv, X.; Han, D.; Zhang, Q.; Niu, L.; Chen, W. Enhanced Catalytic Performance of Pt-Free Iron Phthalocyanine by Graphene Support for Efficient Oxygen Reduction Reaction. *ACS Catal.* **2013**, *3*, 1263.

(22) Zhang, C.; Hao, R.; Yin, H.; Liu, F.; Hou, Y. Iron phthalocyanine and nitrogen-doped graphene composite as a novel non-precious catalyst for the oxygen reduction reaction. *Nanoscale* **2012**, *4*, 7326.

(23) Sun, D.; Shen, Y.; Zhang, W.; Yu, L.; Yi, Z.; Yin, W.; Wang, D.; Huang, Y.; Wang, J.; Wang, D.; Goodenough, J. B. A Solution-Phase Bifunctional Catalyst for Lithium−Oxygen Batteries. *J. Am. Chem. Soc.* **2014**, *136*, 8941.

(24) El-Barbary, A. A.; Telling, R. H.; Ewels, C. P.; Heggie, M. I.; Briddon, P. R. Structure and energetics of the vacancy in graphite. *Phys. Rev. B: Condens. Matter Mater. Phys.* **2003**, *68*, 144107.

(25) Lee, G.-D.; Wang, C. Z.; Yoon, E.; Hwang, N.-M.; Kim, D.-Y.; Ho, K. M. Diffusion, Coalescence, and Reconstruction of Vacancy Defects in Graphene Layers. *Phys. Rev. Lett.* **2005**, *95*, 205501.

(26) Kotakoski, J.; Mangler, C.; Meyer, J. C. Imaging atomic-level random walk of a point defect in graphene. *Nat. Commun.* **2014**, *5*, 3991.

(27) Banhart, F.; Kotakoski, J.; Krasheninnikov, A. V. Structural Defects in Graphene. *ACS Nano* **2011**, *5*, 26.

(28) Wang, Y.; Li, X.; Yang, J. Electronic and magnetic properties of CoPc and FePc molecules on graphene: the substrate, defect, and hydrogen adsorption effects. *Phys. Chem. Chem. Phys.* **2019**, *21*, 5424.

(29) Chen, Y.; Hua, X.; Chen, S. Theoretical study of stability of metal-N4 macrocyclic compounds in acidic media. *Chin. J. Catal.* **2016**, *37*, 1166.

(30) Cortés-Arriagada, D.; Miranda-Rojas, S.; Cid-Mora, F.; Toro-Labbé, A. First-principles study of hybrid nanostructures formed by

https://doi.org/10.1021/acsomega.2c05170
ACS Omega 2022, 7, 43915−43922

deposited phthalocyanine/porphyrin metal complexes on phosphorene. *J. Mol. Liq.* **2021**, *333*, 115948.
(31) Basiuk, V. A.; Chávez-Colorado, E. Adsorption of free-base phthalocyanine on Stone-Wales defect-containing carbon nanotubes: A DFT study. *Diamond Relat. Mater.* **2019**, *97*, 107443.
(32) Feng, S.; Luo, N.; Tang, A.; Chen, W.; Zhang, Y.; Huang, S.; Dou, W. Phthalocyanine and Metal Phthalocyanines Adsorbed on Graphene: A Density Functional Study. *J. Phys. Chem. C* **2019**, *123*, 16614.
(33) Kresse, G.; Furthmüller, J. Efficiency of ab-initio total energy calculations for metals and semiconductors using a plane-wave basis set. *Comput. Mater. Sci.* **1996**, *6*, 15.
(34) Kresse, G.; Furthmüller, J. Efficient iterative schemes for ab initio total-energy calculations using a plane-wave basis set. *Phys. Rev. B: Condens. Matter Mater. Phys.* **1996**, *54*, 11169.
(35) Perdew, J. P.; Burke, K.; Ernzerhof, M. Generalized Gradient Approximation Made Simple. *Phys. Rev. Lett.* **1996**, *77*, 3865.
(36) Blöchl, P. E. Projector augmented-wave method. *Phys. Rev. B: Condens. Matter Mater. Phys.* **1994**, *50*, 17953.
(37) Dudarev, S. L.; Botton, G. A.; Savrasov, S. Y.; Humphreys, C. J.; Sutton, A. P. Electron-energy-loss spectra and the structural stability of nickel oxide: An LSDA+U study. *Phys. Rev. B: Condens. Matter Mater. Phys.* **1998**, *57*, 1505.
(38) Zhou, J.; Sun, Q. Magnetism of Phthalocyanine-Based Organometallic Single Porous Sheet. *J. Am. Chem. Soc.* **2011**, *133*, 15113.
(39) Dou, W.; Huang, S.; Lee, C. Graphene-enhanced intermolecular interaction at interface between copper- and cobalt-phthalocyanines. *J. Chem. Phys.* **2015**, *143*, 134706.
(40) Grimme, S. Semiempirical GGA-type density functional constructed with a long-range dispersion correction. *J. Comput. Chem.* **2006**, *27*, 1787.
(41) Meyer, J. C.; Kisielowski, C.; Erni, R.; Rossell, M. D.; Crommie, M. F.; Zettl, A. Direct Imaging of Lattice Atoms and Topological Defects in Graphene Membranes. *Nano Lett.* **2008**, *8*, 3582.
(42) Ugeda, M. M.; Brihuega, I.; Guinea, F.; Gómez-Rodríguez, J. M. Missing Atom as a Source of Carbon Magnetism. *Phys. Rev. Lett.* **2010**, *104*, 096804.
(43) He, X.; Tang, A.; Li, Y.; Zhang, Y.; Chen, W.; Huang, S. Theoretical studies of SiC van der Waals heterostructures as anodes of Li-ion batteries. *Appl. Surf. Sci.* **2021**, *563*, 150269.
(44) Li, L.; Reich, S.; Robertson, J. Defect energies of graphite: Density-functional calculations. *Phys. Rev. B: Condens. Matter Mater. Phys.* **2005**, *72*, 184109.
(45) Wang, Z.; Zhou, Y. G.; Bang, J.; Prange, M. P.; Zhang, S. B.; Gao, F. Modification of Defect Structures in Graphene by Electron Irradiation: Ab Initio Molecular Dynamics Simulations. *J. Phys. Chem. C* **2012**, *116*, 16070−16079.
(46) Zhang, Z.; Wang, S.; Ding, L.; Liang, X.; Pei, T.; Shen, J.; Xu, H.; Chen, Q.; Cui, R.; Li, Y.; Peng, L.-M. Self-Aligned Ballistic n-Type Single-Walled Carbon Nanotube Field-Effect Transistors with Adjustable Threshold Voltage. *Nano Lett.* **2008**, *8*, 3696−3701.
(47) Kroll, T.; Kraus, R.; Schönfelder, R.; Aristov, V. Y.; Molodtsova, O. V.; Hoffmann, P.; Knupfer, M. Transition metal phthalocyanines: Insight into the electronic structure from soft x-ray spectroscopy. *J. Chem. Phys.* **2012**, *137*, 054306.
(48) Haldar, S.; Bhandary, S.; Vovusha, H.; Sanyal, B. Comparative study of electronic and magnetic properties of iron and cobalt phthalocyanine molecules physisorbed on two-dimensional MoS_2 and graphene. *Phys. Rev. B* **2018**, *98*, 085440.
(49) Manz, T. A.; Sholl, D. S. Chemically Meaningful Atomic Charges that Reproduce the Electrostatic Potential in Periodic and Nonperiodic Materials. *J. Chem. Theory Comput.* **2010**, *6*, 2455−2468.
(50) Chen, H.; Hua, Y.; Luo, N.; He, X.; Li, Y.; Zhang, Y.; Chen, W.; Huang, S. Lithiation Abilities of SiC Bulks and Surfaces: A First-Principles Study. *J. Phys. Chem. C* **2020**, *124*, 7031−7038.

https://doi.org/10.1021/acsomega.2c05170
ACS Omega 2022, 7, 43915−43922